Ocean Sci. Discuss., 11, 1691–1718, 2014
www.ocean-sci-discuss.net/11/1691/2014/
doi:10.5194/osd-11-1691-2014

Ocean Science
Discussions
Open Access

Comparative heat and gas exchange measurements in the Heidelberg Aeolotron, a large annular wind-wave tank

L. Nagel[1], **K. E. Krall**[1], **and B. Jähne**[1,2]

[1]Institute of Environmental Physics, University of Heidelberg, Im Neuenheimer Feld 229, 69120 Heidelberg, Germany
[2]Heidelberg Collaboratory for Image Processing, University of Heidelberg, Speyerer Straße 6, 69115 Heidelberg, Germany

Received: 13 June 2014 – Accepted: 17 June 2014 – Published: 25 June 2014

Correspondence to: B. Jähne (bernd.jaehne@iwr.uni-heidelberg.de)

Published by Copernicus Publications on behalf of the European Geosciences Union.

Abstract

A comparative study of simultaneous heat and gas exchange measurements was performed in the large annular Heidelberg Air–Sea Interaction Facility, the Aeolotron, under homogeneous water surface conditions. The use of two gas tracers, N_2O and C_2HF_5, resulted not only in gas transfer velocities, but also in the measurement of the Schmidt number exponent n with a precision of ±0.025. The original controlled flux or active thermographic technique proposed by Jähne et al. (1989) was applied by heating a large patch at the water surface to measure heat transfer velocities. Heating a large patch, the active thermography technique is laterally homogeneous and problems of lateral transport effects are avoided. Using the measured Schmidt number exponents, the ratio of the scaled heat transfer velocities to the measured gas transfer velocities is 1.046 ± 0.040, a good agreement within the limits of experimental uncertainties. This indicates the possibility to scale heat transfer velocities measured by active thermography to gas transfer velocities, provided the Schmidt number exponent is known and that the heated patch is large enough to reach the thermal equilibrium.

1 Introduction

In 1989 Jähne et al. (1989) proposed to use heat as a proxy tracer for gas transfer velocities, then called the "controlled flux technique" (CFT). This technique provides transfer velocity measurements with high temporal resolution in the order of minutes and spatial resolution of less than a meter. However, using heat as a proxy for mass has one significant drawback. Diffusion of heat is about one hundred times faster than diffusion of mass in water. Because transfer velocities of two different tracers, including heat, scale with their diffusivity, the transfer velocity of a gas k_{gas} can be extrapolated from the transfer velocity of heat k_{heat} by

OSD
11, 1691–1718, 2014

$$k_{gas} = k_{heat}\left(\frac{D_{gas}}{D_{heat}}\right)^{n} = k_{heat}(Le)^{-n}. \quad (1)$$

Le denotes the Lewis number. To be able to use Eq. (1) the exponent n has to be known. The exponent n gradually decreases from 2/3 for a smooth water surface to 1/2 for a wavy surface (Jähne et al., 1987b; Richter and Jähne, 2011). If the water temperature is different as well, Eq. (1) generalizes to

$$k_{gas} = k_{heat}\left(\frac{Sc}{Pr}\right)^{-n}, \quad (2)$$

where the Schmidt number is $Sc = \nu/D_{gas}$ and the Prandtl number is $Pr = \nu/D_{heat}$. By performing simultaneous gas and heat transfer measurements in the Karlsruhe linear air–sea interaction facility, Jähne et al. (1989) validated this extrapolation.

The initial radiometer used by Jähne et al. (1989) was a point measuring device. Once thermal imaging systems with a sufficiently low noise level became available, thermographic techniques evolved into an even more useful method to investigate small-scale air–sea interaction processes. With advanced imaging devices, it was not only possible to measure transfer velocities, but to provide a direct "insight" into the small-scale processes taking place at the ocean surface. Therefore, these imaging devices were used to study the mechanisms determining the transfer of mass across the air–sea interface such as Langmuir circulation (Melville et al., 1998), micro-scale wave breaking (Jessup et al., 1997; Zappa et al., 2001, 2004), surface renewal processes (Zappa et al., 1998), and the surface velocity field (Garbe et al., 2003; Veron et al., 2008).

For field measurements, various modifications of the original CFT were applied (Haußecker et al., 2002). Haußecker et al. (1995) developed a method based on a surface renewal model to track the decay of a small heated spot and applied this technique during the MBL-ARI cruise. However, this modification was not verified by independent

OSD
11, 1691–1718, 2014

laboratory measurements by directly comparing gas transfer and heat transfer velocities.

Schimpf et al. (1999) proposed not to apply an artificial infrared radiation to the surface, but to use the naturally occurring net heat flux instead. By an analysis of the temperature statistics, they estimated the temperature difference across the heat boundary layer at the sea surface. This approach was also based on a surface renewal model and was used in three field campaigns: CoOP 1995, CoOP1997, and GasEx1999 (Schimpf et al., 2004; Frew et al., 2004).

Then, however, experimental evidence became available that indicated that it is not possible to extrapolate from heat transfer velocities to gas transfer velocities using a surface renewal model. During the Fluxes, Air–sea Interactions and Remote Sensing (FAIRS) experiment Asher et al. (2004) measured heat transfer velocities by tracking heated spots and using a surface renewal model, i. e., a Schmidt number exponent $n = 1/2$. Simultaneously, gas transfer velocities were measured during FAIRS. Gas transfer velocities calculated by scaling the measured heat transfer velocities were found to be 2 times as large as the directly measured gas transfer velocities.

Atmane et al. (2004) performed simultaneous gas exchange measurements with He and SF_6 and heat transfer measurements in a 9.1 m long linear wind-wave tank. They found that heat and gas transfer velocities can be well matched using a modification of the surface renewal model, the random eddy model by Harriott (1962), which assumes that the boundary layer is only partly renewed. Later Jessup et al. (2009) provided further evidence for complete and partial surface renewal. The Hariott model also leads to varying Schmidt number exponents. However, this is not the only model with this property. Jähne (1985) showed that the experimentally found variation of the Schmidt number exponent n between 2/3 and 1/2 can be explained by different types of models, either the extended surface renewal model, where the probability for surface renewal depends on the distance to the surface, or the turbulent diffusion model with different assumptions about the increase of the turbulent diffusivity with the distance from the interface.

OSD
11, 1691–1718, 2014

All previous comparisons, however, have one or both of the following two deficits. First, they were performed in linear facilities, where it is difficult to compare the locally measured heat transfer velocity with a gas transfer velocity, which is averaged over the whole facility. Second, all more recent comparisons include only the modification of active thermography with a small heated spot. With this technique, a three-dimensional modeling is actually required, because heat is also being transported horizontally by molecular diffusion and by the shear current in the boundary layer. It is still unclear to which extend these effects influence the measured heat transfer velocity using the spot technique.

The purpose of this investigation is therefore a careful study with simultaneous heat and gas exchange measurements in a wind-wave tank with spatially more homogeneous conditions. Such a facility is the large annular Heidelberg Air–Sea Interaction Facility, the Aeolotron. The original controlled flux developed by Jähne et al. (1989) is applied, where a large patch at the water surface is heated. By heating a large patch, the active thermography technique is laterally homogeneous – provided the patch is large enough – and all problems with lateral transport effects are avoided. This investigation aims to answer the question whether it is possible to scale heat transfer measurements performed with the CFT to gas transfer measurements without any model assumptions, provided the Schmidt number exponent n is known.

2 The wind-wave facility

2.1 The Heidelberg Aeolotron

The Heidelberg Aeolotron is an annular wind-wave facility with a diameter of 8.68 m at the inside wall and a width of 0.61 m (Fig. 1). The annular shape results in a quasi-stationary wave field with a virtually unlimited fetch. For the conducted measurements, deionized water with a height of 1.0 m was used, which corresponds to a water volume of about 17.9 m^3. The air part of the flume above the water has a height of 1.4 m. Wind

OSD
11, 1691–1718, 2014

is generated by two axial fans mounted diametrically in the ceiling of the air space of the flume. The maximum wind speed (scaled to the reference height of 10 m), that can be produced by the wind generator is $u_{10} = 20\,\mathrm{m\,s^{-1}}$.

2.2 Homogeneity of the wind field in the Aeolotron

Because of the geometry of the facility, a logarithmic wind profile is not formed in the Aeolotron. Centrifugal forces due to the curved walls generate secondary currents (Schlichting, 2000). Furthermore, the wind speed is not uniformly distributed throughout the whole facility due to the positions and type of the wind generators. Bopp (2014) showed that the wind speed and therefore also the friction velocity at the measurement location of the thermography setup is $15\% \pm 5\%$ higher than for the average of the whole flume. When comparing locally measured heat transfer velocities with gas transfer velocities, which are integrated over the whole water area, this difference between the local and the averaged wind forcing has to be taken into account.

2.3 Measurement conditions

The measurements were conducted in spring 2010 using six different wind speed conditions between $u_{10} = 2.7\,\mathrm{m\,s^{-1}}$ and $12.7\,\mathrm{m\,s^{-1}}$. Each condition was repeated two or three times. Table 1 summarizes wind speeds and friction velocities for each condition averaged over the three measurement days, as well as the mean water temperatures for each measuring day. All friction velocities used in this study are water-sided. Exact values for the wind speed and the friction velocity can be found in Appendix A for each condition. The wind speed conditions were chosen such that they were roughly equidistant in log space.

OSD
11, 1691–1718, 2014

3 The controlled flux technique

The controlled flux technique inverts classical gas transfer measurements: a known flux density is forced to the water surface and the resulting concentration difference is measured. For the heat exchange measurements, the setup tested in a pilot experiment under field conditions, as described in Schimpf et al. (2011), was used. A carbon dioxide laser (Evolution 100, Synrad Inc.) with an emitting wavelength of $\lambda = 10.6\,\mu m$ creates a heat flux density, which is distributed homogeneously in wind direction over a rectangular area with a mirror scanning system (Micro Max 671, Cambridge Technology Inc.). The temperature response of the water surface is measured with an infrared camera (CMT256, Thermosensorik) with a resolution of 256 pixel × 256 pixel in the wave length regime of $\lambda = 3.4$–$5\,\mu m$ and a noise equivalent temperature difference of less than $\Delta T = 20\,mK$. During each condition, the laser is switched on and off with changing frequencies. This allows a system theoretical approach for data analysis as proposed in Jähne et al. (1989). The thermal boundary layer acts like a low pass filter to the laser forcing. For low forcing frequencies the surface reaches the equilibrium temperature of constant forcing. For higher frequencies the system can not reach the thermal equilibrium, the penetration depth is reduced, resulting in transport which is restricted to molecular diffusion and the temperature response is damped. From the measured temperature response of the system, the transfer function and therefore the cut-off frequency, which corresponds to the response time τ of the system, is determined in the Fourier domain. The transfer velocity is then calculated from the response time by

$$k = \sqrt{\frac{D_{heat}}{\tau}}. \tag{3}$$

The advantage of this data evaluation method is that it is independent on model assumption, that a flux density calibration is not required and the low liability to reflections.

OSD
11, 1691–1718, 2014

4 Gas exchange

To measure gas exchange velocities k_{gas}, a box model method is employed. The wind-wave tank is interpreted as two well mixed boxes. One of these boxes encompasses the air with a volume of V_a and a homogeneous trace gas concentration of c_a, and the other one the water with a volume of V_w and homogeneous tracer concentration c_w. Trace gases can be exchanged between both boxes through the water surface A. Allowing for the possibility of air leaks with a volume flux of $\dot{V}_a$, the transfer velocity k_{gas} can be calculated using the mass balance for the air box by

$$k_{gas} = \frac{V_a}{A} \cdot \frac{\dot{c}_a + \lambda_a c_a}{c_w} \cdot \frac{1}{1 - \alpha c_a / c_w}. \quad (4)$$

The tracer's dimensionless solubility is denoted by α, and the leak rate is defined as $\lambda_a = \dot{V}_a / V_a$. The box model Eq. (4) is only applicable in this form when the concentration of the tracer ambient air is negligible and no water leaks exist. More thorough derivations of the box model equations can be found in Kräuter (2011); Krall (2013) and Mesarchaki et al. (2014).

Measuring time resolved air and water side concentrations allows the measurement of the transfer velocity of a gas using Eq. (4). Additionally, the geometry of the used wind-wave tank needs to be known, as well as the solubility of the trace gas used. Also, the leak rate λ_a needs to be known or measured.

The instrumentation used to measure concentrations in this study as well as the determination of the leak rate and a detailed analysis of the uncertainties of gas transfer velocity are described in Mesarchaki et al. (2014) and Krall (2013). In this study, the trace gases nitrous oxide (N_2O) and pentafluoroethane (C_2HF_5) were used. Their physico-chemical parameters are listed in Table 2.

To measure the Schmidt number exponent n, Schmidt number scaling, see Eq. (2) is applied to two gases. The transfer velocities of two trace gases, k_1 and k_2 with differing Schmidt numbers Sc_1 and Sc_2 are measured simultaneously, and the Schmidt number

OSD
11, 1691–1718, 2014

exponent is then calculated as

$$n = -\frac{\ln(k_1/k_2)}{\ln(Sc_1/Sc_2)}. \quad (5)$$

5 Results and discussion

5.1 Measured heat transfer velocities

Heat and gas transfer velocities were measured during each wind speed condition with a closed air space. The determination of the heat transfer velocities and their uncertainties is described in detail in Nagel (2014). The water-sided friction velocity was measured under the same conditions, but at a different time. The measurement of the friction velocities is described in Bopp (2014). As Bopp (2014) used slightly different wind speeds in his measurements, a cubic relationship between measured wind speed and friction velocity was fitted to the discrete values listed in Bopp (2014). Here, this relationship is used to determine the averaged friction velocity for each condition. For the local heat transfer measurements, the local friction velocity is assumed to be 15 % larger than the averaged one, see Sect. 2.2.

Figure 2 shows the heat transfer velocities plotted against the local friction velocity. For three conditions (# 3 on 26 April 2010, # 3 on 28 April 2010 and # 1 on 30 April 2010), no transfer velocity could be determined, as the fit of the amplitude damping function did not converge due to large scatter in the measured amplitudes.

To use the system theoretical approach for data analysis, it is necessary that a water parcel stays in the heated area for a time that is long enough to reach the thermal equilibrium. Therefore the response time τ has to be smaller than the residence time of a water parcel in the heated patch. This residence time itself is inversely proportional to the surface drift velocity. The surface drift velocity increases proportionally to the wind speed, while the response time decreases approximately with the square of the wind

OSD
11, 1691–1718, 2014

speed. Therefore the required size of the heated area decreases with increasing wind speed. However, the size of the heated area was not changed between the different measurement conditions. For that reason it is likely that the transfer velocity of the first condition at $u_* \approx 0.33\,\mathrm{cm\,s^{-1}}$ is overestimated, because the heated area was too small.

Because the expected response time of the system decreases with increasing wind speed, the used laser forcing frequencies were increased as well. Nevertheless, to determine the response time, it is necessary that the system can reach the thermal equilibrium at the lowest used forcing frequencies. How well the thermal equilibrium is reached at the lowest forcing frequencies influences the accuracy of the determination of the response time. Figures 3 and 4 show two examples of amplitude damping in dependency of the laser forcing frequency recorded under different wind speed conditions. The fit of the amplitude damping curve has a higher accuracy in Fig. 3, where the thermal equilibrium is reached at more than one of the low forcing frequencies. In contrast, the thermal equilibrium is barely reached in Fig. 4, leading to a larger uncertainty in the response time. Therefore, the accuracy of the calculated heat transfer velocities varies significantly.

5.2 Gas transfer velocities and Schmidt number exponent

The gas transfer velocities, which were measured simultaneously with the heat exchange velocities, are shown in Fig. 5 against the friction velocity averaged over the whole facility. The transfer velocity shown is scaled to a Schmidt number of $Sc = 600$ using Schmidt number scaling, see Eq. (2). The Schmidt number exponent n used for scaling was calculated using the measured transfer velocities of both gases, N_2O as well as C_2HF_5, using Eq. (5). Therefore, scaling the measured gas transfer velocities of both gases to $Sc = 600$ yields the same transfer velocity k_{600}. That means, that even though the transfer velocities of two gases were measured in each condition, only one transfer velocity can be shown. For condition # 3 on 26 April 2010, (see Table 1), which was measured as the first condition on that day, no gas transfer velocity could be calculated. During this condition the trace gases were insufficiently mixed into the water

OSD
11, 1691–1718, 2014

leading to spatially varying water side concentration, making the box model which requires homogeneous concentrations, see Sect. 4, no longer applicable.

The measured Schmidt number exponent n is shown in Fig. 6. It shows a smooth transition from $n = 2/3$ for the low wind speeds to $n = 1/2$ for the highest wind speed as described in Sect. 1. The error estimation of the Schmidt number exponent was done with a mean difference approach, resulting in an error of less than 0.025. The measured gas transfer velocities k_{600} as well as the transition of the Schmidt number exponent n from 2/3 to 1/2 are in good agreement with previous studies in wind-wave facilities (Jähne et al., 1987b; Zappa et al., 2001; Nielsen, 2004; Krall, 2013).

5.3 Comparison between measured gas and heat transfer velocities

To compare heat and gas transfer, all measured transfer velocities are scaled to a Schmidt number of $Sc = 600$ by Schmidt number scaling, as described in Sect. 1, Eq. (2) using the measured Schmidt number exponents.

Figure 7 shows the measured transfer velocities for heat and for a gas in dependency of the friction velocity. The shown gas transfer velocities are integrated over the whole facility, while the heat transfer velocities are measured locally. As described in Sect. 2.2, the wind speed and the friction velocity in the measurement region of the local heat transfer measurements are about 15 % higher than the averaged value of the whole facility. Therefore the transfer velocities are measured at different friction velocities, although they are measured simultaneously. The uncertainty for the local friction velocity is about 5 %, while uncertainties of the friction velocity averaged over the whole facility are taken directly from Bopp (2014).

Figure 7 shows the good agreement between the scaled heat and the scaled gas transfer velocities. To quantify the deviation of the scaled heat transfer velocities, Fig. 8 shows them against the simultaneous measured gas transfer velocities, also scaled to $Sc = 600$. The best-fit line shows a slope of 1.20±0.04. That means that the scaled heat transfer velocities are about 20 % higher than the simultaneously measured gas transfer velocities. However, 15 % can be attributed to the difference in the friction velocity of

OSD
11, 1691–1718, 2014

the local compared to the integrated measurements. Therefore the scaled heat transfer velocities and the gas transfer velocities differ just by 1.046 ± 0.04. This is within the conservatively estimated error budget, which contains three different sources of errors:

First, the absolute uncertainty in the Schmidt number exponent n leads to a relative uncertainty for the heat transfer velocity scaled to a gas transfer velocity of

$$\frac{\sigma_k}{k_{\text{gas}}} = \ln\left(\frac{Sc}{Pr}\right)\sigma_n. \tag{6}$$

where σ_k and σ_n are the absolute uncertainties for the transfer velocity and the Schmidt number exponent, respectively. For $\sigma_n = 0.025$ (Fig. 6) and $Sc/Pr \approx 600/7.2$, the relative scaling error is 11 %.

Second, the accuracy of the absolute value of the Schmidt number is about 5 %. Third, the heat transfer velocities were measured at a local friction velocity, which is 15 % ± 5 % higher than the friction velocity averaged over the whole facility. These three contributions lead, linearly added, to a total error of about 20 %.

6 Conclusions and outlook

This study showed, that it is possible to scale heat transfer velocities to gas transfer velocities. The mean deviation found experimentally is a factor of 1.046 ± 0.04. This is well below the possible maximum systematic deviation, conservatively estimated to be 21 %. This result was found by simultaneous gas transfer and heat transfer measurements using the original approach of Jähne et al. (1989), in the large annular Heidelberg Aeolotron wind wave tank. This approach does not depend on any model assumptions about the transfer processes, only the Schmidt number exponent n must be known. This opens up the opportunity to apply this technique to field measurements. However, three issues must be addressed carefully.

First, water parcels at the surface must stay in the heated patch for a time that is longer than the response time τ of the heat transfer across the boundary layer (see

OSD
11, 1691–1718, 2014

Sect. 5.1). This condition is much harder to meet in the field than in a wind-wave facility and requires a platform that is moving with the water.

Second, the Schmidt number exponent n has to be known with a high certainty. All experimental and theoretical evidence suggests that it is varying between 2/3 and 1/2. With an unknown Schmidt number exponent in this range, the uncertainty of scaling from heat transfer to gas transfer is about a factor of two for a Schmidt number of 600. It is even larger for higher Schmidt numbers (tracers such as SF_6, DMS, and most organic volatiles) and lower for lower Schmidt numbers (e. g., He). Recent measurements by Krall (2013) showed that the exponent n does not simply decrease with increasing wind speed, but also depends on the degree of contamination of the water surface with surface active material. Thus the relation between the Schmidt number exponent n and the surface conditions needs to be investigated carefully. Measurements by Zappa et al. (2004) and Jessup et al. (2009) indicate that it might be possible to infer the exponent from the infrared image sequences themselves, because it is possible to analyze micro-scale wave breaking and full/partial surface renewal events from them.

And third, active thermography does not see bubble-induced gas transfer. This is a clear disadvantage for scaling to gas transfer rates for high wind speed conditions. However, it can be turned into a clear advantage for combined gas transfer – heat transfer field campaigns to determine the bubble-induced part of gas transfer.

Appendix A: Measured transfer velocities

Table A1 shows the numerical results of the measurements described above.

Acknowledgements. We would like to thank M. Bopp for fruitful discussions concerning the friction velocity in the Aeolotron. Financial support for this work by the German Federal Ministry of Education and Research (BMBF) joint project “Surface Ocean Processes in the Anthropocene” (SOPRAN, FKZ 03F0611F and 03F0622F) within the international SOLAS project is gratefully acknowledged.

OSD
11, 1691–1718, 2014

References

Asher, W. E., Jessup, A. T., and Atmane, M. A.: Oceanic application of the active controlled flux technique for measuring air–sea transfer velocities of heat and gases, J. Geophys. Res., 109, C08S12, doi:10.1029/2003JC001862, 2004. 1694

Atmane, M. A., Asher, W., and Jessup, A. T.: On the use of the active infrared technique to infer heat and gas transfer velocities at the air–water free surface, J. Geophys. Res., 109, C08S14, doi:10.1029/2003JC001805, 2004. 1694

Bopp, M.: Luft- und wasserseitige Strömungsverhältnisse im ringförmigen Heidelberger Wind-Wellen-Kanal (Aeolotron), Masterarbeit, available at: http://www.ub.uni-heidelberg.de/archiv/16962 (last access: 12 June 2014), 2014. 1696, 1699, 1701

Degreif, K.: Untersuchungen zum Gasaustausch – Entwicklung und Applikation eines zeitlich aufgelösten Massenbilanzverfahrens, Dissertation, available at: http://www.ub.uni-heidelberg.de/archiv/6120 (last access: 12 June 2014), 2006. 1710

Frew, N., Bock, E., Schimpf, U., Hara, T., Haussecker, H., Edson, J., McGillis, W., Nelson, R., McKenna, S., Uz, B., and Jähne, B.: Air–sea gas transfer: its dependence on wind stress, small-scale roughness, and surface films, J. Geophys. Res., 109, C08S17, doi:10.1029/2003JC002131, 2004. 1694

Garbe, C. S., Spies, H., and Jähne, B.: Estimation of surface flow and net heat flux from infrared image sequences, J. Math. Imaging Vis., 19, 159–174, doi:10.1023/A:1026233919766, 2003. 1693

Harriott, P.: A random Eddy modification of the penetration theory, Chem. Eng. Sci., 17, 149–154, doi:10.1016/0009-2509(62)80026-8, 1962. 1694

Haußecker, H., Reinelt, S., and Jähne, B.: Heat as a proxy tracer for gas exchange measurements in the field: principles and technical realization, in: Air–Water Gas Transfer: Selected Papers from the Third International Symposium on Air–Water Gas Transfer, edited by: Jähne, B. and Monahan, E. C., 24–27 July 1995, Heidelberg, Germany, 405–413, doi:10.5281/zenodo.10401, 1995. 1693

Haußecker, H., Schimpf, U., Garbe, C. S., and Jähne, B.: Physics from IR image sequences: quantitative analysis of transport models and parameters of air–sea gas transfer, in: Gas Transfer at Water Surfaces, edited by: Saltzman, E., Donelan, M., Drennan, W., and Wanninkhof, R., Vol. 127 of Geophysical Monograph, American Geophysical Union, 103–108, doi:10.1029/GM127p0103, 2002. 1693

OSD
11, 1691–1718, 2014

Jähne, B.: Transfer processes across the free water interface, Habilitation thesis, available at: http://www.ub.uni-heidelberg.de/archiv/16798, (last access: 12 June 2014) 1985. 1694
Jähne, B., Heinz, G., and Dietrich, W.: Measurement of the diffusion coefficients of sparingly soluble gases in water, J. Geophys. Res., 92, 10767–10776, doi:10.1029/JC092iC10p10767, 1987a. 1709
Jähne, B., Münnich, K. O., Bösinger, R., Dutzi, A., Huber, W., and Libner, P.: On the parameters influencing air-water gas exchange, J. Geophys. Res., 92, 1937–1950, doi:10.1029/JC092iC02p01937, 1987b. 1693, 1701
Jähne, B., Libner, P., Fischer, R., Billen, T., and Plate, E. J.: Investigating the transfer process across the free aqueous boundary layer by the controlled flux method, Tellus B, 41, 177–195, doi:10.1111/j.1600-0889.1989.tb00135.x, 1989. 1692, 1693, 1695, 1697, 1702
Jessup, A. T., Zappa, C. J., and Yeh, H. H.: Defining and quantifying microscale wave breaking with infrared imagery, J. Geophys. Res., 102, 23145–23153, 1997. 1693
Jessup, A. T., Asher, W. E., Atmane, M., Phadnis, K., Zappa, C. J., and Loewen, M. R.: Evidence for complete and partial surface renewal at an air–water interface, Geophys. Res. Lett., 36, 1–5, doi:10.1029/2009GL038986, 2009. 1694, 1703
Kestin, J., Sokolov, M., and Wakeham, W. A.: Viscosity of liquid water in the range −8 °C to 150 °C, J. Phys. Chem. Ref. Data, 7, 941–948, doi:10.1063/1.555581, 1978. 1709
Krall, K. E.: Laboratory Investigations of Air–Sea Gas Transfer under a Wide Range of Water Surface Conditions, Dissertation, available at: http://www.ub.uni-heidelberg.de/archiv/14392 (last access: 12 June 2014), 2013. 1698, 1701, 1703, 1709, 1711
Kräuter, C.: Aufteilung des Transferwiderstands zwischen Luft und Wasser beim Austausch flüchtiger Substanzen mittlerer Löslichkeit zwischen Ozean und Atmosphäre, Diplomarbeit, available at: http://www.ub.uni-heidelberg.de/archiv/13010 (last access: 12 June 2014), 2011. 1698
Melville, W. K., Shear, R., and Veron, F.: Laboratory measurements of the generation and evolution of Langmuir circulations, J. Fluid Mech., 364, 31–58, doi:10.1017/S0022112098001098, 1998. 1693
Mesarchaki, E., Kräuter, C., Krall, K. E., Bopp, M., Helleis, F., Williams, J., and Jähne, B.: Measuring air–sea gas exchange velocities in a large scale annular wind-wave tank, Ocean Sci. Discuss., 11, 1643–1689, doi:10.5194/osd-11-1643-2014, 2014. 1698

OSD
11, 1691–1718, 2014

Nagel, L.: Active Thermography to Investigate Small-Scale Air–Water Transport Processes in the Laboratory and the Field, Dissertation, available at: http://www.ub.uni-heidelberg.de/archiv/16831 (last access: 12 June 2014), 2014. 1699

Nielsen, R.: Gasaustausch – Entwicklung und Ergebnis eines schnellen Massenbilanzverfahrens zur Messung der Austauschparameter, Dissertation, available at: http://www.ub.uni-heidelberg.de/archiv/5032 (last access: 12 June 2014), 2004. 1701

Richter, K. and Jähne, B.: A laboratory study of the Schmidt number dependency of air-water gas transfer, in: Gas Transfer at Water Surfaces 2010, edited by: Komori, S., McGillis, W., and Kurose, R., 322–332, available at: http://hdl.handle.net/2433/156156 (last access: 12 June 2014), 2011. 1693

Schimpf, U., Haußecker, H., and Jähne, B.: Studies of air–sea gas transfer and micro turbulence at the ocean surface using passive thermography, in: The Wind-Driven Air–Sea Interface: Electromagnetic and Acoustic Sensing, Wave Dynamics and Turbulent Fluxes, edited by: Banner, M. L., 1999. 1694

Schimpf, U., Garbe, C., and Jähne, B.: Investigation of transport processes across the sea surface microlayer by infrared imagery, J. Geophys. Res., 109, C08S13, doi:10.1029/2003JC001803, 2004. 1694

Schimpf, U., Nagel, L., and Jähne, B.: First results of the 2009 SOPRAN active thermography pilot experiment in the Baltic Sea, in: Gas Transfer at Water Surfaces 2010, edited by: Komori, S., McGillis, W., and Kurose, R., 358–367, available at: http://hdl.handle.net/2433/156156 (last access: 12 June 2014), 2011. 1697

Schlichting, H.: Boundary Layer Theory, 8th Edn., Springer, 2000. 1696

Tamimi, A., Rinker, E. B., and Sandall, O. C.: Diffusion coefficients for hydrogen sulfide, carbon dioxide, and nitrous oxide in water over the temperature range 293–368 K, J. Chem. Eng. Data, 39, 330–332, doi:10.1021/je00014a031, 1994. 1709

Veron, F., Melville, W. K., and Lenain, L.: Wave-coherent air–sea heat flux, J. Phys. Oceanogr., 38, 788–802, doi:10.1175/2007JPO3682.1, 2008. 1693

Weiss, R. F.: Carbon dioxide in water and seawater: the solubility of a non-ideal gas, Mar. Chem., 2, 203–215, doi:10.1016/0304-4203(74)90015-2, 1974. 1709

Yaws, C. L.: Diffusion coefficient in water – organic compounds, in: Transport Properties of Chemicals and Hydrocarbons, chap. 12, 502–593, doi:10.1016/B978-0-8155-2039-9.50017-X, 2009. 1709

OSD
11, 1691–1718, 2014

Young, C. L. (Ed.): IUPAC Solubility Data Series: Oxides of Nitrogen, Vol. 8, Pergamon Press, Oxford, England, 1981. 1709

Zappa, C. J., Jessup, A. T., and Yen, H.: Skin layer recovery of free-surface wakes: Relation to surface renewal and dependence on heat flux and background turbulence, J. Geophys. Res., 103, 21711–21721, doi:10.1029/98JC01942, 1998. 1693

Zappa, C. J., Asher, W. E., and Jessup, A. T.: Microscale wave breaking and air-water gas transfer, J. Geophys. Res., 106, 9385–9391, doi:10.1029/2000JC000262, 2001. 1693, 1701

Zappa, C. J., Asher, W. E., Jessup, A. T., Klinke, J., and Long, S. R.: Microbreaking and the enhancement of air-water transfer velocity, J. Geophys. Res., 109, C08S16, doi:10.1029/2003JC001897, 2004. 1693, 1703

OSD

11, 1691–1718, 2014

Table 1. Measurement conditions used in this study. Shown are the mean friction velocities u_* and the wind speeds u_{10} averaged over the three measurement days, as well as the mean water temperatures for each day, T_{mean}. The conditions at which measurements were conducted on each day are marked with an x.

cond. #	1	2	3	4	5	6	
u_* averaged [cm s^{-1}]	0.283	0.370	0.511	0.707	1.086	1.713	
u_{10} averaged [m s^{-1}]	2.74	3.51	4.69	6.24	8.90	12.66	T_{mean} [°C]
26 Apr 2010	x		x		x		20.1
28 Apr 2010	x	x	x	x	x	x	20.5
30 Apr 2010	x	x	x	x	x	x	20.8

OSD
11, 1691–1718, 2014

Table 2. Chemical and physical properties of the trace gases used, nitrous oxide (N_2O) and pentafluoroethane (C_2HF_5), as well as for carbon dioxide (CO_2) for comparison. All values are given at 20 °C for fresh water.

Formula	M $g\,mol^{-1}$	α	D $10^{-5}\,cm^2\,s^{-1}$	Sc
N_2O	44.01	0.59[a]	1.63[b]	613
C_2HF_5	120.02	0.45 [c]	0.97[d]	1031
CO_2	44.01	0.94[e]	1.67[f]	599

[a] Young (1981) [b] Tamimi et al. (1994), [c] Krall (2013), [d] Yaws (2009), [e] Weiss (1974), [f] Jähne et al. (1987a).
Given Schmidt numbers are calculated using $Sc = \nu/D$ with $\nu = 0.010\,cm^2\,s^{-1}$ (Kestin et al., 1978).

OSD
11, 1691–1718, 2014

Table A1. Measured response times τ, heat transfer velocities k_{heat}, transfer velocities and Schmidt numbers of N_2O and the Schmidt number exponents n in dependency of wind speed u_{10} and the water-sided friction velocity u_*. The Prandtl number of heat was $Pr = 7.2$ under all measured conditions. The temperature dependent Schmidt number of N_2O was taken from Degreif (2006).

date	u_{10} [m s^{-1}] averaged	u_* [cm s^{-1}] averaged	u_* [cm s^{-1}] local	τ [s]	k_{heat} [cm h^{-1}]	k_{N_2O} [cm h^{-1}]	Sc N_2O	n
26 Apr 2010	2.78	0.288	0.332	2.079 ± 0.520	94.74 ± 11.51	2.13 ± 0.22	597	0.66
28 Apr 2010	2.73	0.283	0.326	2.270 ± 0.259	90.67 ± 5.03	2.93 ± 0.35	586	0.65
30 Apr 2010	2.69	0.279	0.321	–	–	3.22 ± 0.49	575	0.64
28 Apr 2010	3.53	0.373	0.429	2.108 ± 0.726	94.08 ± 15.75	4.29 ± 0.46	585	0.62
30 Apr 2010	3.48	0.367	0.422	2.807 ± 0.310	81.54 ± 4.37	4.97 ± 0.64	572	0.59
26 Apr 2010	4.70	0.512	0.589	–	–	–	598	–
28 Apr 2010	4.71	0.513	0.590	–	–	6.94 ± 0.67	585	0.60
30 Apr 2010	4.68	0.509	0.585	2.463 ± 4.834	87.05 ± 83.06	7.70 ± 0.87	573	0.57
28 Apr 2010	6.26	0.711	0.817	0.535 ± 0.196	186.85 ± 33.28	14.32 ± 1.61	584	0.57
30 Apr 2010	6.21	0.704	0.809	0.491 ± 0.348	194.97 ± 67.17	14.77 ± 1.71	573	0.57
26 Apr 2010	8.91	1.088	1.251	0.160 ± 0.085	341.55 ± 88.06	26.67 ± 2.64	597	0.50
28 Apr 2010	8.92	1.089	1.253	0.101 ± 0.024	430.15 ± 49.27	32.79 ± 3.22	584	0.55
30 Apr 2010	8.87	1.082	1.244	0.089 ± 0.041	458.57 ± 102.8	30.21 ± 3.21	573	0.55
28 Apr 2010	12.67	1.715	1.972	0.055 ± 0.010	583.12 ± 51.69	51.38 ± 4.84	584	0.53
30 Apr 2010	12.66	1.712	1.969	0.060 ± 0.009	556.95 ± 42.42	46.67 ± 4.40	573	0.51

OSD
11, 1691–1718, 2014

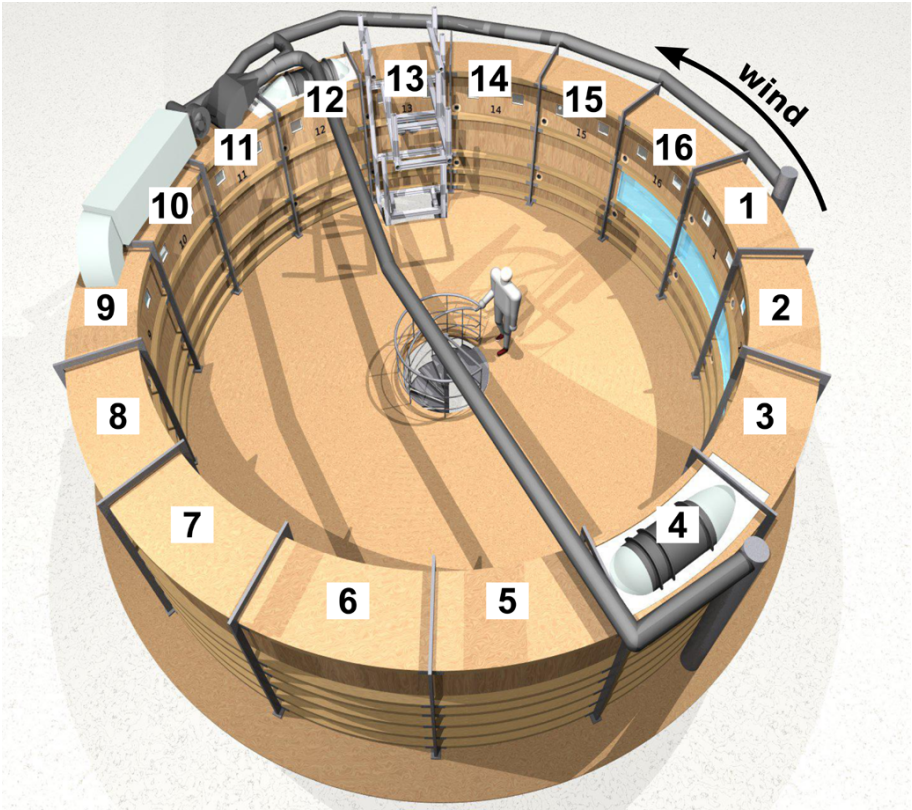

Figure 1. Rendered view of the Aeolotron, taken from Krall (2013). The 16 segments are numbered clockwise, while the wind direction is counter-clockwise. The wind generating fans can be seen in segments 4 and 12. The heat transfer velocity is measured in segment 13, while the gas transfer measurements integrate over the whole water surface.

OSD
11, 1691–1718, 2014

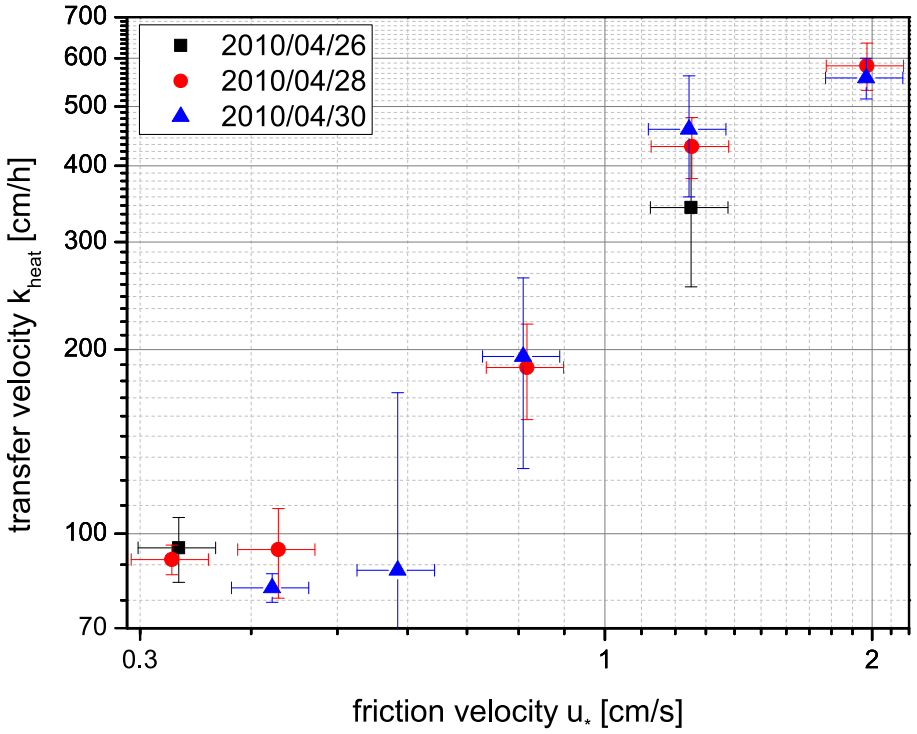

Figure 2. Measured heat transfer velocities plotted against the locally measured friction velocity.

OSD
11, 1691–1718, 2014

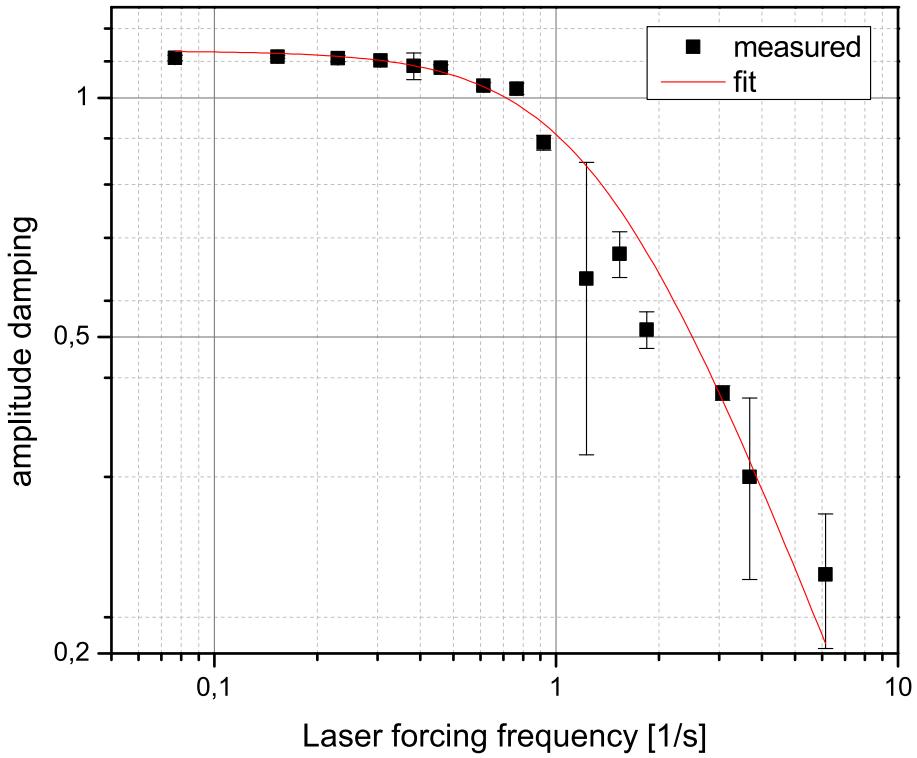

Figure 3. Example for measured amplitude damping plotted against the laser forcing frequency at a friction velocity of $u_* = 0.28\,\mathrm{cm\,s^{-1}}$. At low forcing frequencies the thermal equilibrium was easily reached.

OSD
11, 1691–1718, 2014

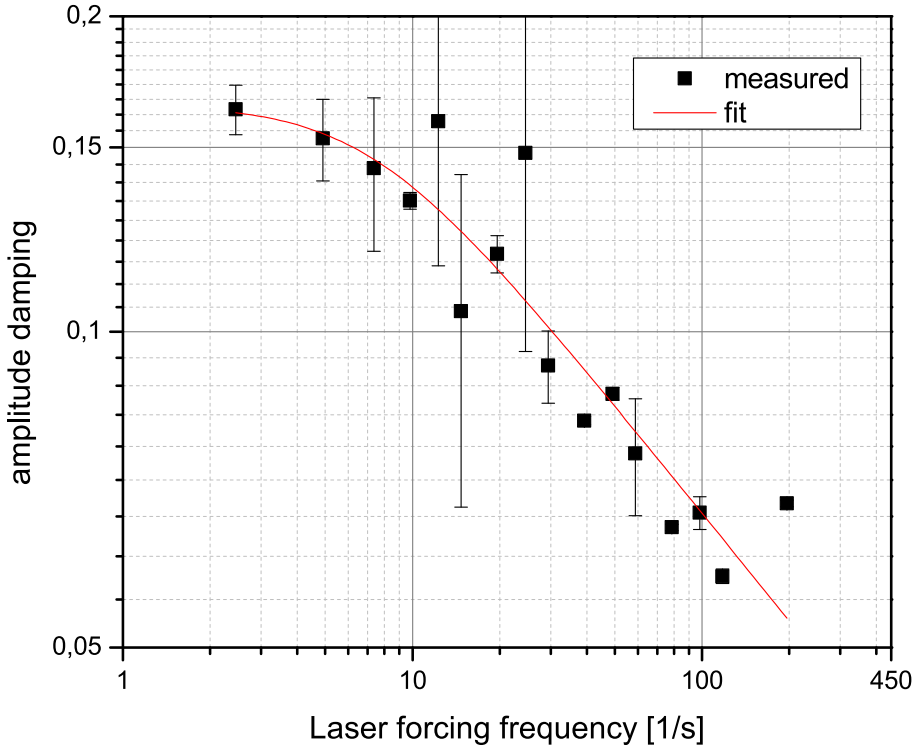

Figure 4. Example for measured amplitude damping plotted against of the laser forcing frequency at a friction velocity of $u_* = 2.46\,\mathrm{cm\,s^{-1}}$. At low forcing frequencies the thermal equilibrium was barely reached.

OSD
11, 1691–1718, 2014

Scaling CFT heat transfer velocities to gas transfer velocities

L. Nagel et al.

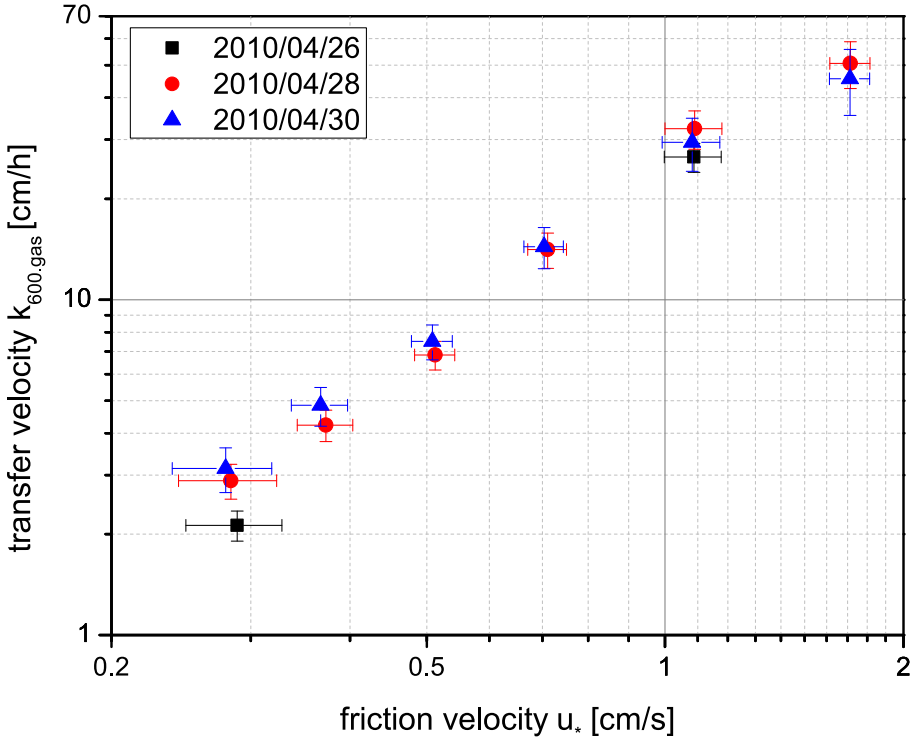

Figure 5. Measured gas transfer velocities scaled to a Schmidt number of $Sc = 600$ plotted against the global averaged friction velocity.

OSD
11, 1691–1718, 2014

Scaling CFT heat transfer velocities to gas transfer velocities

L. Nagel et al.

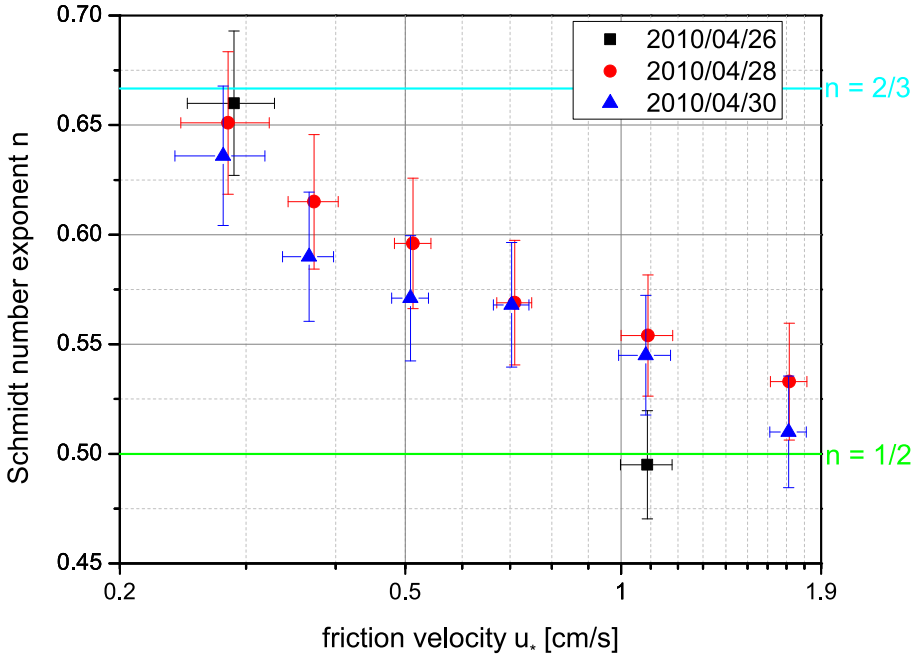

Figure 6. Measured Schmidt number exponents n with an error of 5 % plotted against the global averaged friction velocity u_*.

OSD
11, 1691–1718, 2014

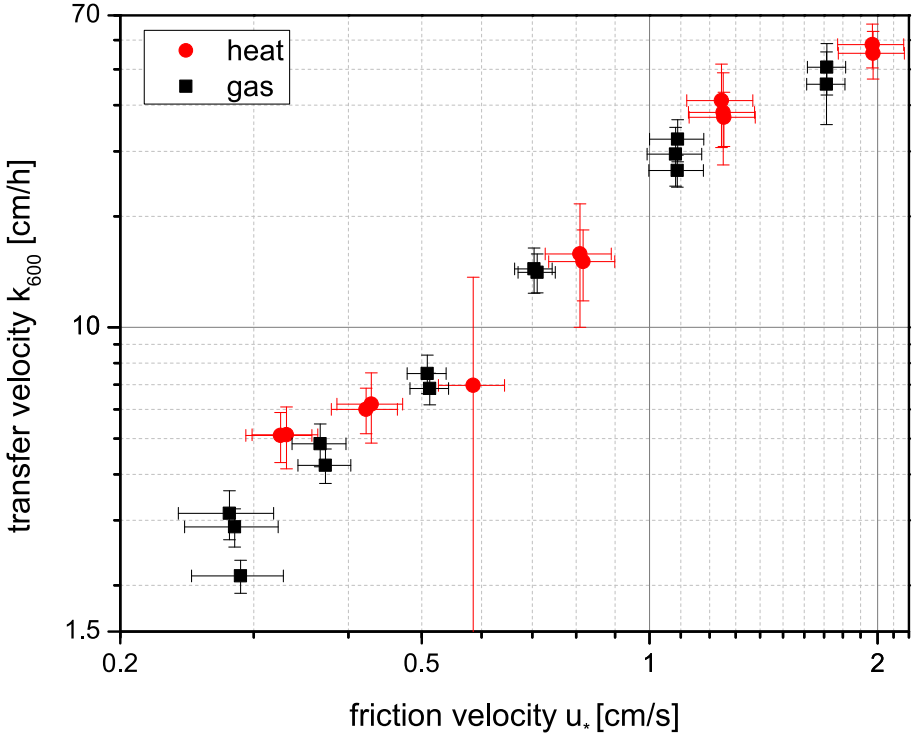

Figure 7. Simultaneously measured heat and gas transfer velocities, both scaled to a Schmidt number of $Sc = 600$ plotted against of the friction velocity.

OSD
11, 1691–1718, 2014

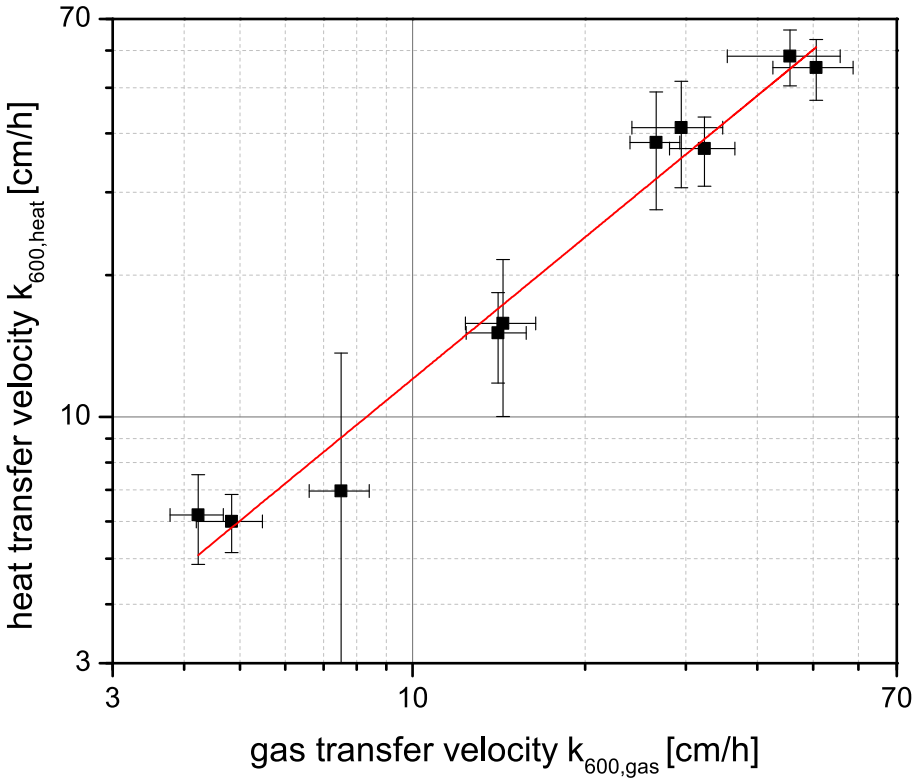

Figure 8. Heat transfer velocities plotted against simultaneously measured gas transfer velocities, both scaled to a Schmidt number of $Sc = 600$. The best-fit line has a slope of 1.20 ± 0.04.

OSD
11, 1691–1718, 2014